Nuclear Medicine and Biology 66 (2018) 10–17

Contents lists available at ScienceDirect

Nuclear Medicine and Biology

journal homepage: www.elsevier.com/locate/nucmedbio

Effects of adding an albumin binder chain on [^{177}Lu]Lu-DOTATATE

Etienne Rousseau [a,b,1], Joseph Lau [a,1], Zhengxing Zhang [a], Carlos F. Uribe [a], Hsiou-Ting Kuo [a], Chengcheng Zhang [a], Jutta Zeisler [a], Nadine Colpo [a], Kuo-Shyan Lin [a,c,*], François Bénard [a,c,*]

[a] Department of Molecular Oncology, BC Cancer Research Centre, Vancouver, BC V5Z 1L3, Canada
[b] Département de Médecine Nucléaire et Radiobiologie, Université de Sherbrooke, Sherbrooke, QC J1H 5N4, Canada
[c] Department of Radiology, University of British Columbia, Vancouver, BC V5Z 1M9, Canada

ARTICLE INFO

Article history:
Received 30 April 2018
Received in revised form 9 July 2018
Accepted 7 August 2018

Keywords:
Peptide receptor radionuclide therapy
Albumin binder
Neuroendocrine tumour
DOTATATE
Therapy
Dosimetry

ABSTRACT

Introduction: [^{177}Lu]Lu-DOTATATE peptide receptor radionuclide therapy is used for treatment of neuroendocrine tumours. We investigated whether prolonging blood residence time of [^{177}Lu]Lu-DOTATATE with albumin binders could increase tumour accumulation and tumour-to-kidney ratios for improved therapeutic efficacy.
Methods: DOTATATE and its derivatives with an albumin-binder motif (GluAB-DOTATATE and AspAB-DOTATATE) were prepared by solid-phase peptide synthesis. Binding affinities of the Lu-labeled peptides for human somatostatin receptor 2 (SSTR2) were measured with membrane competition binding assays. Compounds were radiolabeled with [^{177}Lu]$LuCl_3$ and purified by HPLC. SPECT imaging and biodistribution studies (1, 4, 24, 72, and 120 h) were performed in immunodeficient mice bearing AR42J pancreatic tumour xenografts.
Results: GluAB-DOTATATE and AspAB-DOTATATE were synthesized in 18.8% and 14.3% yields, while Lu-GluAB-DOTATATE and Lu-AspAB-DOTATATE were obtained in 86.5% and 50.0% yields, respectively. The compounds exhibited nanomolar binding affinity (K_i: 8.72–8.95 nM) for SSTR2. The ^{177}Lu-labeled peptides were obtained in non-decay-corrected isolated yields of ≥41%, with >96% radiochemical purity, and molar activities in the range of 314–497 GBq/μmol. In vivo, [^{177}Lu]Lu-GluAB-DOTATATE and [^{177}Lu]Lu-AspAB-DOTATATE had significantly higher blood activity at 1, 4 and 24 h compared to [^{177}Lu]Lu-DOTATATE. Tumour uptake of [^{177}Lu]Lu-DOTATATE was 21.35 ± 5.90%ID/g at 1 h and decreased to 10.10 ± 5.78%ID/g at 120 h. For [^{177}Lu]Lu-GluAB-DOTATATE tumour uptake increased from 21.89 ± 6.86%ID/g at 1 h to 24.44 ± 5.84%ID/g at 4 h, before decreasing to 12.02 ± 1.84%ID/g at 120 h. For [^{177}Lu]Lu-AspAB-DOTATATE tumour uptake was 11.12 ± 3.18%ID/g at 1 h, 18.41 ± 4.36% ID/g at 24 h, and decreased to 16.90 ± 8.97%ID/g at 120 h. Renal uptake was 7.49 ± 1.62%ID/g for [^{177}Lu]Lu-DOTATATE, 31.14 ± 7.06%ID/g for [^{177}Lu]Lu-GluAB-DOTATATE, and 28.82 ± 13.82%ID/g for [^{177}Lu]Lu-AspAB-DOTATATE at 1 h and decreased thereafter.
Conclusion: The addition of albumin binder motifs to [^{177}Lu]Lu-DOTATATE enhanced mean residence time in blood. Increased tumour uptake was observed for [^{177}Lu]Lu-AspAB-DOTATATE compared to [^{177}Lu]Lu-DOTATATE at later time points, but its higher kidney uptake diminished the therapeutic index.

1. Introduction

Gastroenteropancreatic neuroendocrine tumours (GEP-NETs), initially described as carcinoids ("karzinoide") by Oberndofer in 1907, are a heterogeneous group of rare tumours originating from tissues derived from APUD cells and that are characterized by high rates of metastatic disease on initial diagnosis and sometimes florid clinical presentations secondary to their secretion of neurotransmitters and hormones [1–4]. NETs are characterized by the overexpression of somatostatin receptors (SSTRs). The advent of somatostatin analogues coupled with radiometal chelators has enabled the delivery of beta-emitting radionuclides to SSTR2 expressing cells in a targeted manner with peptide receptor radionuclide therapy (PRRT) [5–7]. For agonists, there is internalization of the compound and since ^{177}Lu is a residualizing radionuclide, it remains trapped within the cell [8]. Advantages of the technique include rarity of severe toxicity (0.6% hepatic insufficiency, 0.8% myelodysplastic syndrome, 0.4% renal insufficiency) for patients and good control of disease (24%–46% overall response rate), especially for [^{177}Lu]Lu-DOTATATE [2,5,7].

In the case of ^{177}Lu-labeled somatostatin analogues the dose-limiting organ is the kidney, followed by the bone marrow [6]. The ratio of tumour dose to kidney dose can be defined as the therapeutic index and a higher index is advantageous because the dose that can be delivered to the tumour is then higher for the same kidney toxicity. The uptake mechanism is related to expression of somatostatin

* Corresponding authors at: Department of Molecular Oncology, BC Cancer Research Centre, 675 West 10th Avenue, Vancouver, BC V5Z 1L3, Canada.
E-mail addresses: klin@bccrc.ca (K.-S. Lin), fbenard@bccrc.ca (F. Bénard).
[1] Co-first authors.

https://doi.org/10.1016/j.nucmedbio.2018.08.001
0969-8051/

receptors 1–5 in normal kidneys, but high uptake is also attributable to reabsorption by proximal tubules of the peptides filtered by the glomeruli. This reabsorption pathway can be partially blocked by intravenous infusion of cationic amino acid, as previously reported [9–13]. Even though healthy and tumour tissue express the receptor, differences in expression levels and in tissue-specific pharmacokinetics can allow for a useful therapeutic index.

For patients with somatostatin-expressing tumours, PRRT has become a useful treatment modality that can target disease not amenable to surgical excision. Although this technique has shown good results in clinical trials, we hypothesize that the pharmacokinetics of DOTATATE, most notably its rapid blood clearance (<10%ID in blood at 3 h), can be enhanced to facilitate higher tumour binding [14]. Albumin binding is a strategy that has been employed to increase blood residence time of a variety of compounds including long-lived insulin derivatives like Levemir and chemotherapeutic drugs like Abraxane [15]. Several techniques have been explored to exploit albumin binding including in vitro/in vivo covalent conjugation and in vitro/in vivo non-covalent human serum albumin binding. For example, Müller et al. reported the use of albumin binders to develop radiopharmaceutical agents targeting folate receptor for cancer imaging and therapy [16]. Herein, we investigated the use of two albumin binders to increase bioavailability of [^{177}Lu]Lu-DOTATATE derivatives, to reduce renal accumulation, and to deliver higher radiation dose to tumour.

2. Materials and methods

2.1. Reagents and equipment

All reagents and solvents were purchased from commercial sources and used without further purification. Peptides were synthesized on an AAPPTec (Louisville, KY) Endeavor 90 peptide synthesizer. High performance liquid chromatography (HPLC) was performed on an Agilent (Santa Clara, CA) 1260 infinity system equipped with a model 1200 quaternary pump, a model 1200 UV absorbance detector (set at 220 nm), and a Bioscan (Washington, DC) NaI scintillation detector. The HPLC columns used were a semi-preparative column (Luna C18, 5 μ, 250 × 10 mm) and an analytical column (Luna C18, 5 μ, 250 × 4.6 mm) both purchased from Phenomenex (Torrance, CA). Mass analyses were performed using an AB SCIEX (Framingham, MA) 4000 QTRAP mass spectrometer system with an ESI ion source. [^{177}Lu]$LuCl_3$ was purchased from ITG (Munich, Germany). Activity of ^{177}Lu-labeled peptides was measured using a Capintec (Ramsey, NJ) CRC®-25R/W dose calibrator, and the activity of mouse tissues collected from biodistribution studies were counted using a Perkin Elmer (Waltham, MA) Wizard2 2480 automatic gamma counter.

2.2. Synthesis of precursor and standards

The peptide octreotate (TATE) was synthesized according to literature procedure using standard Fmoc-based solid-phase peptide synthesis [17]. TATE-coupled resin was then treated with 20% piperidine (15 mL × 2) in DMF to remove the N^{α}-Fmoc protecting group. Three equivalents of Fmoc-Lys(IvDde)-OH, Fmoc-Glu(^{t}Bu)-OH (for GluAB-DOTATATE) or Fmoc-Asp(^{t}Bu)-OH (for AspAB-DOTATATE), and 4-(*p*-Iodophenyl)butyric acid, pre-activated with HBTU/HOBT/DIEA in a ratio of 3/3/6 were subsequently coupled to the sequence. N^{ε}-(ivDde) protecting group was removed by incubating with 1% hydrazine monohydrate in DMF. Three equivalents of tri-tert-butyl 1,4,7,10-tetraazacyclododecane-1,4,7,10-tetraacetate (DOTA-Tris(*t*-Bu ester)) pre-activated with HBTU/DIEA (3/20) were then coupled to the lysine N^{ε}-side chain. The desired albumin binder and DOTA conjugated TATE peptides were cleaved from the resin and simultaneously deprotected by incubating with TFA/TIS/DI water/thioanisole/phenol (82.5/2.5/5/5/5) cocktail solution. The purification of both peptides was performed on HPLC with the semi-preparative column under a flow rate of 4.5 mL/min. The HPLC conditions are summarized in Table 1.

Lutetium chelated non-radioactive standards of GluAB-DOTATATE and AspAB-DOTATATE were prepared by incubating the corresponding peptide with 5 equivalents of $LuCl_3$ in 0.5 mL 0.1 M NaOAc buffer (pH 4.5) at 100 °C for 15 min. At the end of the incubation period, the reaction mixtures were purified by HPLC using the semi-preparative column under a flow rate of 4.5 mL/min. The HPLC conditions are summarized in Table 1.

2.3. Radiolabeling

For radiolabeling, 15–30 μL of [^{177}Lu]$LuCl_3$ containing activity between 388.5 MBq to 654.9 MBq were added into a solution of 25 μg of the corresponding albumin binder and DOTA conjugated TATE peptide in NaOAc buffer (0.5 mL, 0.1 M, pH 4.5). The reaction mixture was incubated at 100 °C for 15 min. Following incubation, the reaction mixtures were injected to HPLC for purification (to separate the radiotracer from free [^{177}Lu]$LuCl_3$ and unlabeled precursor) with the semi-preparative column under a flow rate of 4.5 mL/min. Quality control, including determination of molar activity, was performed on HPLC using the analytical column under a flow rate of 2 mL/min. The HPLC conditions and radiochemistry data are summarized in Table 2.

2.4. Binding affinity

The binding affinities of Lu-DOTATATE, Lu-GluAB-DOTATATE, and Lu-AspAB-DOTATATE to SSTR2 were determined using a membrane-based competition binding assay per published procedures [17]. Purified CHO-K1 membranes (25 μg/well) overexpressing human SSTR2 (Perkin Elmer, Waltham, MA) were incubated with [^{125}I]I-Tyr^{11}-somatostatin-14 (0.05 nM, Perkin Elmer) and competing non-radioactive ligands (10 μM to 1 pM) in a 96-well, 1.2 μm glass fibre filter plate (EMD Millipore, Darmstadt, Germany). The plates were pre-incubated with 0.1% polyethylenimine for 1 h at room temperature. The membrane, radioligand and competing peptides were diluted in assay buffer (25 mM HEPES, pH 7.4, 10 mM $MgCl_2$, 1 mM $CaCl_2$, 0.5% BSA) and incubated for 1 h at 27 °C with moderate shaking. Following the incubation period, the mixture was aspirated through the filters, followed by 6 washes with 200 μL ice-cold wash buffer (50 mM Tris–HCl pH 7.4, 0.2% BSA). Each filter was removed and counted on a gamma counter. Each assay plate contained triplicates and assays were repeated three times for each radiotracer. The inhibition constants (K_i) were calculated by fitting the data to a one-site Fit-Ki curve in GraphPad Prism 7 (GraphPad Software, Inc., La Jolla, CA). The values are reported as mean ± standard deviation, with the reported standard deviation values representing inter-assay variations.

Table 1
HPLC purification conditions, chemical yield and mass-spec analysis of precursors and standards.

Peptide	HPLC solvent	Retention time (min)	Yield %	Molecular formula	M^+ calculated	M^+ found
GluAB-DOTATATE	31% MeCN (0.1% TFA), 69% water (0.1% TFA)	20.4	18.8	$C_{86}H_{118}IN_{17}O_{24}S_2$	1963.7	$[M + 2H]^{2+}$ 983.0
AspAB-DOTATATE	32% MeCN (0.1% TFA), 68% water (0.1% TFA)	15.3	14.3	$C_{85}H_{116}IN_{17}O_{24}S_2$	1949.7	$[M + 2H]^{2+}$ 975.8
Lu-GluAB-DOTATATE	31% MeCN (0.1% TFA), 69% water (0.1% TFA)	24.3	86.5	$C_{86}H_{115}ILuN_{17}O_{24}S_2$	2136.6	$[M + H + Na]^{2+}$ 1080.4
Lu-AspAB-DOTATATE	32% MeCN (0.1% TFA), 68% water (0.1% TFA)	19.5	50.0	$C_{85}H_{113}ILuN_{17}O_{24}S_2$	2121.6	$[M + 2H]^{2+}$ 1061.8

Table 2
HPLC conditions and radiochemical properties of ^{177}Lu-labeled pharmaceuticals.

Peptide	HPLC solvent	Retention time (min)	% isolated radiochemical yield	% purity	Molar activity (GBq/μmol)
[^{177}Lu]Lu-DOTATATE	21% MeCN (0.1% TFA), 79% water (0.1% TFA)	17.0 (purification), 6.7 (QC)	68–73 ($n = 2$)	>99%	384.8–492.1 ($n = 2$)
[^{177}Lu]Lu-GluAB-DOTATATE	31% MeCN (0.1% TFA), 69% water (0.1% TFA)	24.3 (purification), 9.2 (QC)	46–54 ($n = 2$)	>96%	310.8–318.2 ($n = 2$)
[^{177}Lu]Lu-AspAB-DOTATATE	32% MeCN (0.1% TFA), 68% water (0.1% TFA)	18.5 (purification), 7.1 (QC)	40–42 ($n = 2$)	>99%	440.3–555.0 ($n = 2$)

2.5. Cell culture

The AR42J exocrine/pancreas *Rattus norvegicus* cell line (ATCC CRL-1492) was chosen as a tumour model because of its known expression of the SSTR2 receptor [8]. Cells were cultured in a 5% CO_2 atmosphere at 37 °C in a humidified incubator with F-12 K medium (Life Technologies Corporations, Grand Island, NY) supplemented with 20% fetal bovine serum (Sigma-Aldrich, St. Louis, MO), 100 I.U./mL penicillin, and 100 μg/mL streptomycin (Penicillin-Streptomycin Solution, Life Technologies). Prior to inoculation, cells were harvested by trypsinization (Life Technologies), washed, and re-suspended in Dulbecco's Phosphate Buffered Saline (D-PBS) (Life Technologies) to a concentration of 5×10^6 or 10×10^6 cells/50 μL D-PBS and then added to an equal volume of Matrigel (Corning Matrigel Matrix, Bedford, MA).

2.6. Animal model

All animal work was done in accordance with guidelines established by the Canadian Council on Animal Care and approved by the Animal Ethics Committee of the University of British Columbia. Male NOD.Cg-Rag1^{tm1Mom} Il2rg^{tm1Wjl}/SzJ mice were kept in a pathogen-free environment under a 12 h light/dark cycle in the Animal Resource Centre, BC Cancer Research Centre, Vancouver, Canada. Under inhalant anesthesia (2.0%–2.5% Isoflurane in 2.0 L/min oxygen), they were inoculated subcutaneously on the right flank with 100 μL of the AR42J/D-PBS/Matrigel solution and tumours were allowed to grow for 2 to 3 weeks before biodistribution and/or imaging studies.

Each mouse intended for biodistribution was injected intravenously under inhalant anesthesia on day-0 with 3.11 ± 1.56 MBq of radiopharmaceutical, while those meant for imaging received 39.2 ± 4.65 MBq. The injected mass was $7.09 \times 10^{-12} \pm 3.76 \times 10^{-12}$ mol for [^{177}Lu]Lu-DOTATATE, $9.89 \times 10^{-12} \pm 4.96 \times 10^{-12}$ for [^{177}Lu]Lu-GluAB-DOTATATE, and $6.25 \times 10^{-12} \pm 3.30 \times 10^{-12}$ for [^{177}Lu]Lu-AspAB-DOTATATE.

2.7. Biodistribution

For each time-point (1, 4, 24, 72, and 120 h after radiopharmaceutical injection), after anesthesia with isoflurane, the mice were sacrificed by CO_2 inhalation followed by cardiac puncture; urine released at the time of death was collected. Organs/tissues were harvested, rinsed with D-PBS, blotted dry, weighed, and their activity was assayed by gamma counter with a counting time of 1 min per tube. Resulting counts per minute from the gamma counter were converted to MBq using a previously determined calibration curve and the percentage injected dose per gram of tissue (%ID/g) was calculated by dividing organ activity by injected dose and organ weight.

2.8. Imaging

Imaging of [^{177}Lu]Lu-DOTATATE, [^{177}Lu]Lu-GluAB-DOTATATE, and [^{177}Lu]Lu-AspAB-DOTATATE injected mice was done under isoflurane anesthesia, after dorsal subcutaneous injection of 250 μL to 500 μL of sterile physiological saline for hydration, on an animal U-SPECT-II/CT scanner (MILabs, Utrecht, Netherlands) using the Ultrahigh resolution multi-pinhole rat-mouse (1 mm pinhole size) collimator. Image acquisition duration was 30 min for the 1 and 4 h post-injection time-points and 60 min for the 24, 72, and 120 h time-points. CT acquisition was done using 615 μA and 60 kV parameters. SPECT acquisition was performed in list mode with a 20% width energy window centered at 210 keV. Background windows of 20% width centered at 171.5 keV and 257.0 keV were also set for correction. Image reconstruction was done with the ordered subset expectation maximization (OSEM) algorithm using 16 subsets, 3 iterations, and 0.4 mm voxel size. A 1.0 mm FWHM Gaussian filter was applied post-reconstruction. Images were obtained in NIfTI format, converted into DICOM format and analyzed with Inveon Research Workplace software (Siemens Healthineers, USA). Calibration of image values in %ID/cc (%ID/g) was achieved by converting raw counts/mL from images into MBq/mL using a calibration factor derived from imaging a phantom of known activity (as assayed by dose calibrator).

2.9. Dosimetry

Internal dosimetry estimates for the mice were done using the organ level internal dose assessment (OLINDA) software v.2.0 (Hermes Medical Solution, Stockholm, Sweden) [18]. These calculations were performed using the 25 g mouse MOBY phantom [19]. These models are available in OLINDA but require the input of total number of decays normalized by injected activity in units of MBq*h/MBq for each of the source organ/tumour.

The biodistribution data (available in Supplementary Tables 1–3) was used to determine the kinetic input values required by OLINDA. First, each of the values was decayed to its corresponding time point (the values on the tables are shown at injection time). Then the different time-points of the uptake data (%ID/g) for each organ were fitted to both mono-exponential ($\frac{\%ID}{g} = ae^{-bt}$) and bi-exponential ($\frac{\%ID}{g} = ae^{-bt} + ce^{-dt}$) functions using in-house software developed in Python (Python Software Foundation version 3.5). The best fit was selected based on the coefficient of determination (R^2) of the fit and the residuals. The area under the curve was analytically calculated based on the parameters obtained from the best fit of each organ. Multiplying the integral from the last step by the mass of the organ provided the kinetic input values required by OLINDA. The values for the masses of the organs were the default ones from the phantoms and can be found in reference [19].

The mouse phantom does not model the adrenals, blood, fat, muscle, and seminal vesicles. These organs were grouped together, based on the fraction of mass to the total body, and were included in what OLINDA calls the *remainder of the body*. The biodistribution data includes the intestines but does not differentiate between large and small intestine as the MOBY phantom does. It was assumed that these two regions had the same uptake as the intestines from the biodistribution. Lastly, the number of decays in the tumours was also calculated based on the biodistribution data of the mice. Tumour dosimetry was based on the unit density sphere model described in [20] available in OLINDA.

2.10. Statistical methods

All statistics and graphs were computed using GraphPad Prism 7 or R version 3.4.0 (The R Foundation for Statistical Computing). The threshold for statistical significance was chosen as $p < 0.05$. Time-points were

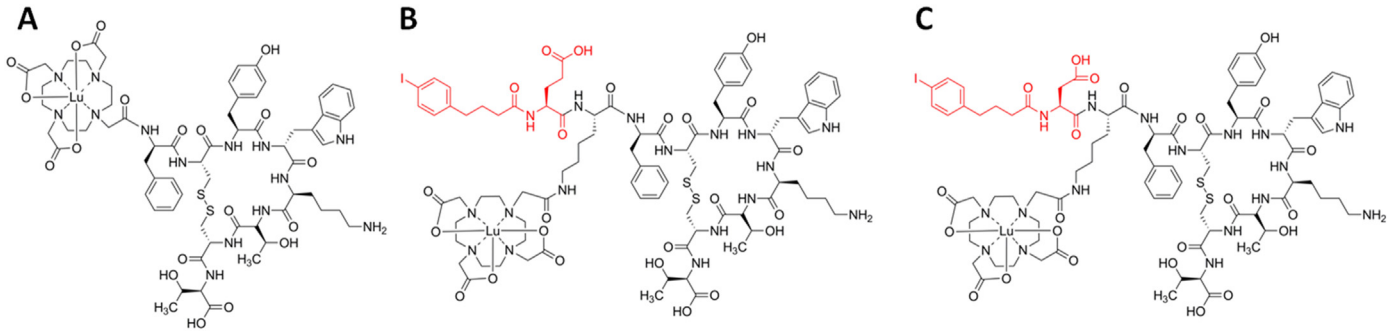

Fig. 1. Chemical structures of (A) Lu-DOTATATE, (B) Lu-GluAB-DOTATATE, and (C) Lu-AspAB-DOTATATE. The albumin binder moiety is highlighted in red.

compared separately. Shapiro's test was used to determine normality (significance level of $\alpha = 0.01$). When data for a given organ at a given time-point was normally distributed for all groups, Welch's *t*-test was used or, if it was not the case, the nonparametric Wilcoxon's rank sum test was used. The *p*-values in each time-point/organ pair were adjusted for multiple comparisons using Holm's method.

Grubb's test was used to identify outliers (significance level of $\alpha = 0.01$). Mice with three or more outliers were removed from analysis entirely ($n = 2$). Outliers attributable to likely urinary contamination during dissection (seminal glands, $n = 4$; muscle, $n = 2$) or to hollow organ contents (stomach, $n = 4$; intestine, $n = 2$) were removed. K_i values were compared by one-way ANOVA in GraphPad.

3. Results

3.1. Peptide synthesis, binding affinity, and radiochemistry

GluAB-DOTATATE and AspAB-DOTATATE were successfully synthesized by solid phase support in 18.8% and 14.3% yields, respectively, while the corresponding standards Lu-GluAB-DOTATATE and Lu-AspAB-DOTATATE were obtained in 86.5% and 50.0% yields, respectively (Fig. 1). The molecular weights of the compounds were confirmed via mass spectrometry (Table 1).

The binding affinities of Lu-GluAB-DOTATATE and Lu-AspAB-DOTATATE for SSTR2 were determined using a cell membrane

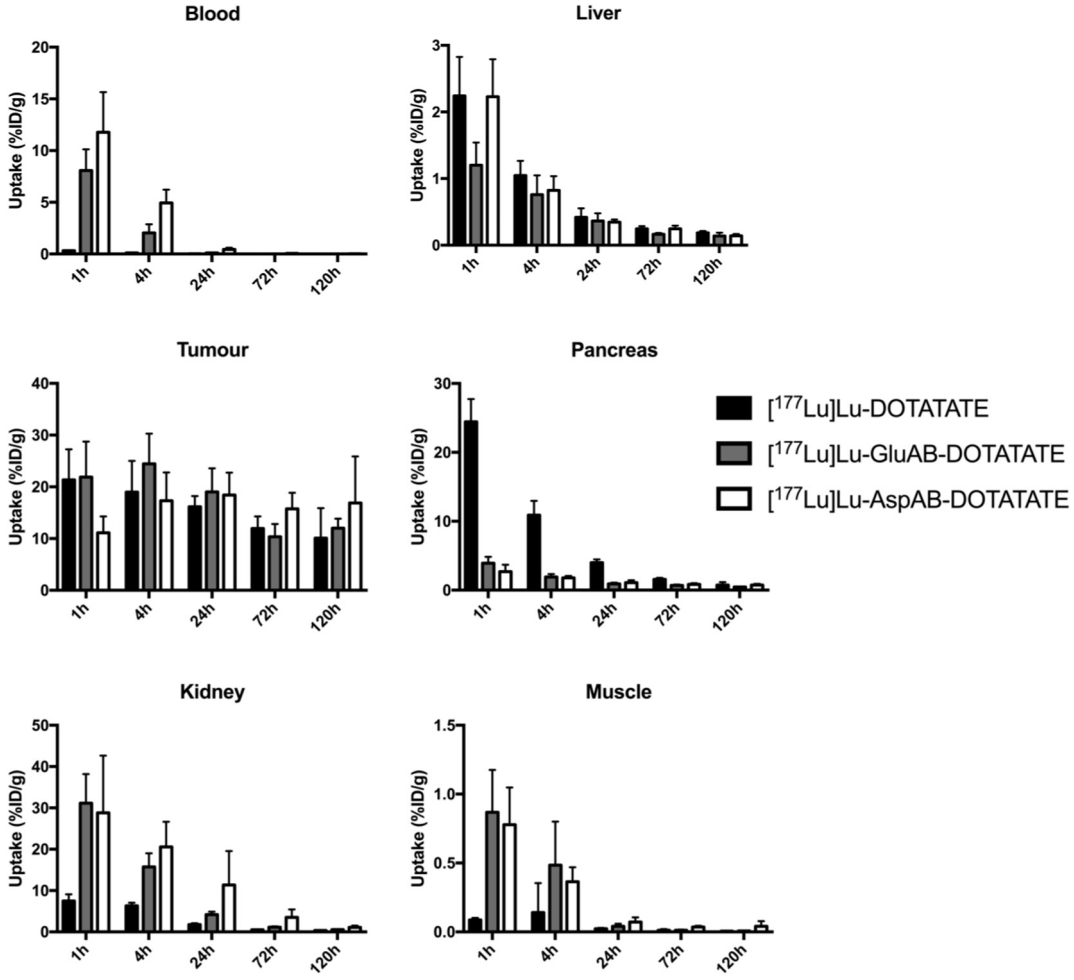

Fig. 2. Radiopharmaceutical biodistribution in blood, tumour, kidney, liver, pancreas and muscle at selected time-points.

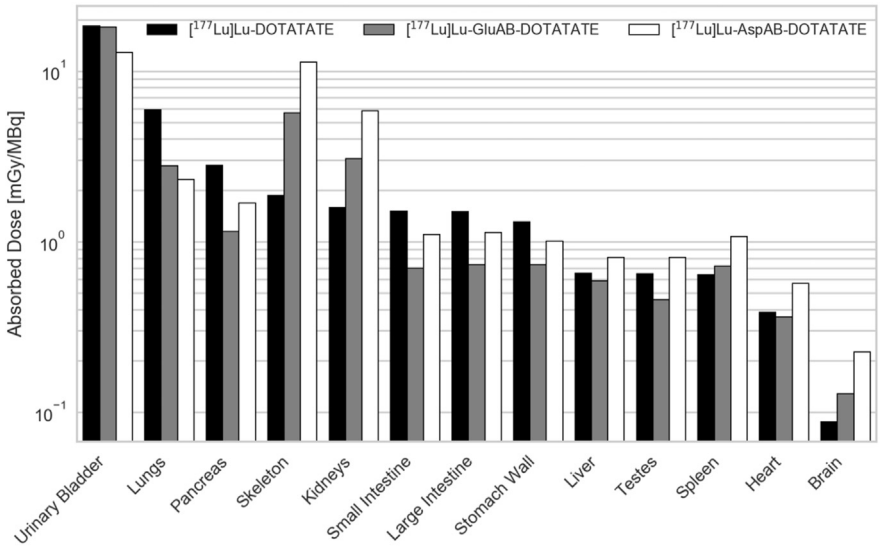

Fig. 3. Absorbed doses per unit of injected activity in organs for the ^{177}Lu-labeled radiopharmaceuticals.

competition assay with [^{125}I]I-Tyr^{11}-somatostatin-14 as the competing ligand. The K_i value for Lu-DOTATATE (3.84 ± 0.30 nM) was lower than Lu-GluAB-DOTATATE (8.95 ± 3.40 nM) and Lu-AspAB-DOTATATE (8.72 ± 3.35 nM), but the differences were not statistically significant.

Radiolabeling data is summarized in Table 2. Tracers were prepared with average non-decay-corrected isolated yields of ≥41.1%. The molar activities measured (reported as range) were 384.8–492.1, 310.8–318.2, and 440.3–555.0 GBq/μmol for [^{177}Lu]Lu-DOTATATE, [^{177}Lu]Lu-GluAB-DOTATATE, and [^{177}Lu]Lu-AspAB-DOTATATE, respectively as measured by HPLC analysis using UV absorption at λ = 220 nm. After HPLC purification, tracers were obtained in >96% average radiochemical purity for in vivo experiments.

3.2. Biodistribution

Comprehensive biodistribution results are summarized in Supplemental Tables 1–3, with organs of interest highlighted in Fig. 2. For tracers with albumin binders, there was significantly higher blood retention compared with the reference compound [^{177}Lu]Lu-DOTATATE (except for [^{177}Lu]Lu-GluAB-DOTATATE at 120 h). [^{177}Lu]Lu-AspAB-DOTATATE had the highest blood uptake at 1, 4, and 24 h (11.77 ± 3.88%ID/g, 4.95 ± 1.27%ID/g, and 0.45 ± 0.15%ID/g respectively), which was significant against [^{177}Lu]Lu-DOTATATE (0.32 ± 0.03%ID/g, 0.11 ± 0.05%ID/g, and 0.03 ± 0.01%ID/g respectively) ($p < 0.01$) and [^{177}Lu]Lu-GluAB-DOTATATE (8.08 ± 2.05%ID/g, 2.05 ± 0.83%ID/g, and 0.10 ± 0.04%ID/g respectively) ($p < 0.05$). At 72 and 120 h, blood uptake was negligible for all tracers (<0.1%ID/g). Bone uptake was only significantly higher in [^{177}Lu]Lu-GluAB-DOTATATE (1.10 ± 0.39%ID/g) compared with [^{177}Lu]Lu-DOTATATE (0.64 ± 0.24%ID/g) at the 1 h time-point ($p < 0.05$). [^{177}Lu]Lu-AspAB-DOTATATE uptake was significantly higher ($p < 0.05$) than that of [^{177}Lu]Lu-DOTATATE at 72 h (0.26 ± 0.05 vs 0.15 ± 0.08%ID/g) and 120 h (0.32 ± 0.22 vs 0.06 ± 0.05%ID/g).

Tumour uptake of [^{177}Lu]Lu-DOTATATE peaked at 1 h (21.35 ± 5.90%ID/g) and decreased to 10.10 ± 5.78%ID/g at 120 h over the course of the study. For [^{177}Lu]Lu-GluAB-DOTATATE tumour uptake increased from 21.89 ± 6.86%ID/g at 1 h to 24.44 ± 5.90%ID/g at 4 h, before decreasing to 12.02 ± 1.84%ID/g at 120 h. [^{177}Lu]Lu-AspAB-DOTATATE tumour uptake was 11.12 ± 3.18%ID/g at 1 h, and progressively increased to 17.33 ± 5.45%ID/g at 4 h, to 18.41 ± 4.36 at 24 h before decreasing to 15.76 ± 3.11 and 16.90 ± 8.97 at 72 and 120 h, respectively. Differences between tumour uptake was only statistically significant for [^{177}Lu]Lu-AspAB-DOTATATE vs [^{177}Lu]Lu-GluAB-DOTATATE and [^{177}Lu]Lu-DOTATATE at 1 h ($p < 0.05$), and for [^{177}Lu]Lu-AspAB-DOTATATE vs [^{177}Lu]Lu-GluAB-DOTATATE at 72 h ($p < 0.05$).

Kidney uptake of the [^{177}Lu]Lu-AspAB-DOTATATE was significantly higher than that of [^{177}Lu]Lu-DOTATATE at all time-points ($p < 0.01$) while that of the [^{177}Lu]Lu-GluAB-DOTATATE was significantly higher only at the 1 h and 4 h time-points ($p < 0.01$). All three tracers displayed similar dynamics with renal uptake highest at 1 h time-point (7.49 ± 1.62%ID/g for [^{177}Lu]Lu-DOTATATE, 31.14 ± 7.06%ID/g for [^{177}Lu]Lu-GluAB-DOTATATE, and 28.82 ± 13.82%ID/g for [^{177}Lu]Lu-AspAB-DOTATATE) and decreasing over time. While ≤1.16%ID/g was observed for [^{177}Lu]Lu-DOTATATE and [^{177}Lu]Lu-GluAB-DOTATATE at 72 h, the renal uptake for [^{177}Lu]Lu-AspAB-DOTATATE was 3.54 ± 1.91%ID/g at the same time-point.

Liver uptake of [^{177}Lu]Lu-AspAB-DOTATATE was higher than other tracers at all time-points. Overall, uptake in that organ was low with the highest value at the 1 h time-point for [^{177}Lu]Lu-AspAB-DOTATATE (2.24 ± 0.58%ID/g).

Pancreas uptake of [^{177}Lu]Lu-DOTATATE was significantly higher than that of other compounds at all time-points ($p < 0.0001$) except at 120 h. The difference was very marked and, in particular, at 1 h, uptake was 24.44 ± 3.30%ID/g, 3.90 ± 0.93, and 2.68 ± 1.01, respectively for [^{177}Lu]Lu-DOTATATE, [^{177}Lu]Lu-GluAB-DOTATATE, and [^{177}Lu]Lu-AspAB-DOTATATE.

Table 3
Organ doses in mSv/MBq for the mice based on the 25 g mouse phantom available in OLINDA v.2.0.

Target organ	[^{177}Lu] Lu-DOTATATE	[^{177}Lu] Lu-GluAB-DOTATATE	[^{177}Lu] Lu-AspAB-DOTATATE
Brain	8.80E−02	1.28E−01	2.25E−01
Large intestine	1.50E+00	7.33E−01	1.13E+00
Small intestine	1.51E+00	7.01E−01	1.10E+00
Stomach wall	1.31E+00	7.34E−01	1.01E+00
Heart	3.85E−01	3.61E−01	5.70E−01
Kidneys	1.59E+00	3.07E+00	5.84E+00
Liver	6.53E−01	5.91E−01	8.09E−01
Lungs	5.93E+00	2.78E+00	2.32E+00
Pancreas	2.80E+00	1.15E+00	1.69E+00
Skeleton	1.87E+00	5.70E+00	1.13E+01
Spleen	6.41E−01	7.22E−01	1.07E+00
Testes	6.47E−01	4.56E−01	8.11E−01
Thyroid	1.25E−01	1.79E−01	3.12E−01
Urinary bladder	1.84E+01	1.82E+01	1.29E+01
Remainder of the body	5.03E−01	4.19E−01	6.10E−01

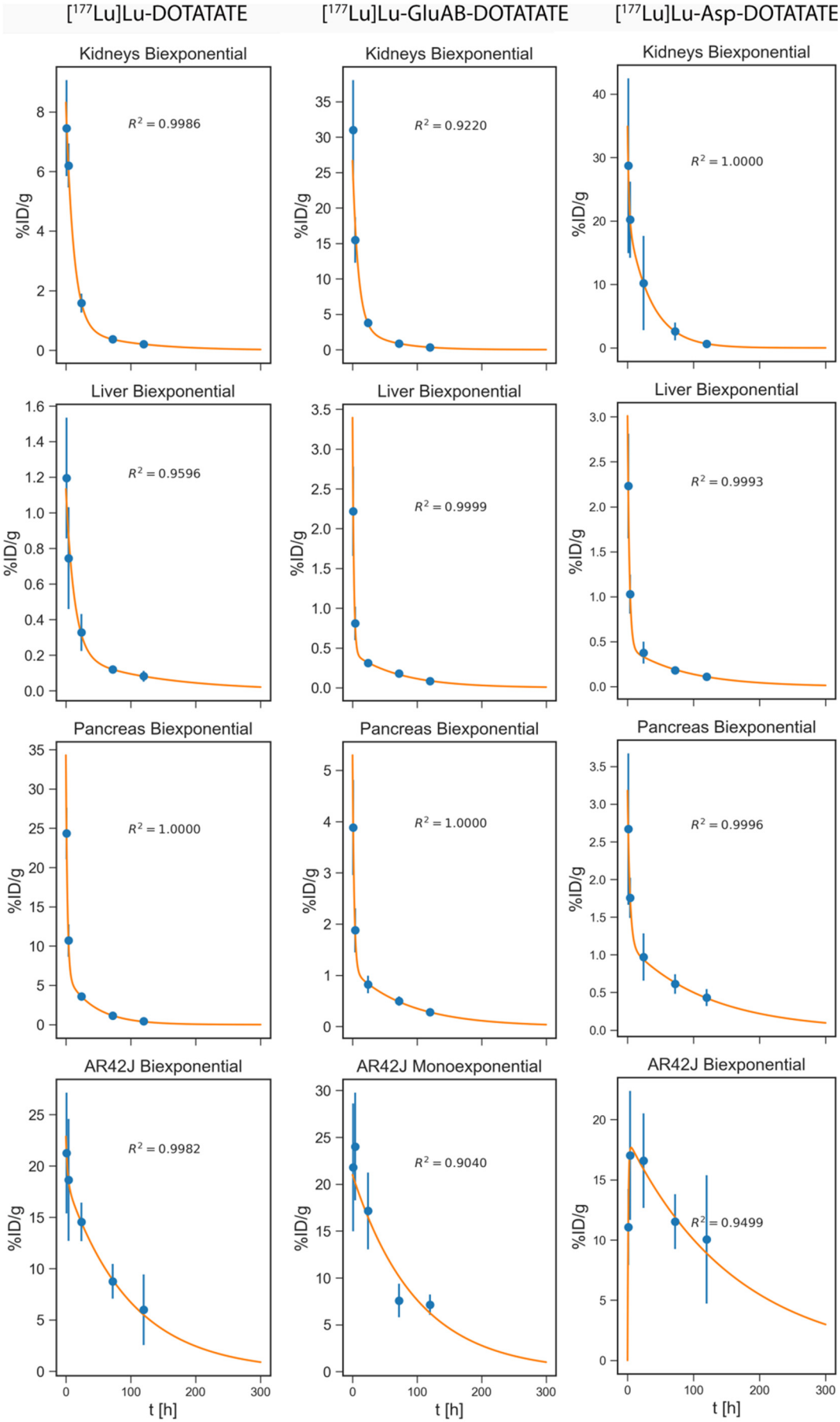

Fig. 4. Uptake of the ^{177}Lu-labeled radiopharmaceuticals as a function of time for kidneys, liver, pancreas and AR42J tumours. The total number of decays per unit injected dose is calculated by multiplying the area under the curve by the phantom organ mass. The y-axis is percentage injected dose per gram of tissue (%ID/g) and the x-axis is time.

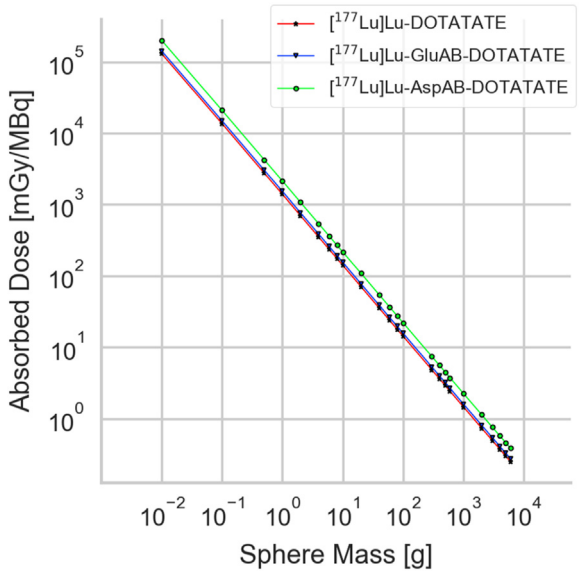

Fig. 5. Absorbed doses per unit of injected activity in AR42J tumours based on unit density sphere model as a function of mass for the ^{177}Lu-labeled radiopharmaceuticals.

3.3. Dosimetry based on biodistribution data

Calculations with OLINDA software are shown in Fig. 3 and Table 3, derived from kinetic curves obtained via biodistribution (Fig. 4). The kidney dose of [^{177}Lu]Lu-GluAB-DOTATATE (3.07 mSv/MBq) and [^{177}Lu]Lu-AspAB-DOTATATE (5.84 mSv/MBq) was higher than that of [^{177}Lu]Lu-DOTATATE (1.59 mSv/MBq). Dose to the skeleton (mostly secondary to blood activity in the marrow) was also higher in [^{177}Lu]Lu-GluAB-DOTATATE (5.70 mSv/MBq) and [^{177}Lu]Lu-AspAB-DOTATATE (11.3 mSv/MBq) compared with [^{177}Lu]Lu-DOTATATE (1.87 mSv/MBq). This was expected because of increased blood residence of the radiolabeled compounds that bind to albumin. The organ that received the highest dose for the mouse model was the urinary bladder (12.9–18.4 mSv/MBq) because that is the main route of excretion.

Based on unit density sphere model (Fig. 5), [^{177}Lu]Lu-GluAB-DOTATATE and [^{177}Lu]Lu-AspAB-DOTATATE were able to deliver 1.10 and 1.54 fold higher dose to AR42J tumours for the same injected activity as [^{177}Lu]Lu-DOTATATE. However, this translated to higher dose delivered to kidney compared to [^{177}Lu]Lu-DOTATATE (1.93 and 3.67 fold, respectively) for [^{177}Lu]Lu-GluAB-DOTATATE and [^{177}Lu]Lu-AspAB-DOTATATE.

4. Discussion

The aim of the present study was to add an albumin binder moiety to a ^{177}Lu-labeled somatostatin analogue to increase blood residence time with the hypothesis that increased bioavailability would increase tumour uptake with less effect on kidney dose. To achieve this, we conjugated Lys-Glu-4-(*p*-iodophenyl)butyric acid or Lys-Asp-4-(*p*-iodophenyl)butyric acid to the base compound DOTATATE to synthesize GluAB-DOTATATE and AspAB-DOTATATE, respectively (Fig. 1). Compared to previously published albumin binders, the albumin binders in this study were designed to be compatible with solid phase peptide synthesis strategy. Beyond DOTATATE, the facile synthesis of these two albumin binders could aid in the development of other radiopharmaceuticals. Non-radioactive standards were prepared and cell competition binding assays were conducted to determine binding affinity of the prospective radiopharmaceuticals to SSTR2. While Lu-DOTATATE had the highest binding affinity (3.84 ± 0.30 nM), the incorporation of an albumin binder did not significantly affect SSTR2 receptor binding in vitro as Lu-GluAB-DOTATATE (8.95 ± 3.40 nM) and Lu-AspAB-DOTATATE (8.72 ± 3.35 nM) retained binding affinities in the nanomolar range.

We proceeded to evaluate the in vivo targeting properties of [^{177}Lu]Lu-GluAB-DOTATATE and [^{177}Lu]Lu-AspAB-DOTATATE in mice bearing AR42J exocrine/pancreas xenografts (Fig. 6). In our experiments, both albumin binders increased blood residence time of the radiopharmaceuticals compared with [^{177}Lu]Lu-DOTATATE. However, this did not translate into the wanted effect of increasing the therapeutic index. Sustained increased tumour uptake compared with [^{177}Lu]Lu-DOTATATE was only observed for [^{177}Lu]Lu-AspAB-DOTATATE (16.90 ± 8.97 vs 10.10 ± 5.78%ID/g at 120 h), but its higher kidney uptake (31.14 ± 7.09 vs 7.49 ± 1.62%ID/g) diminished the therapeutic index, thus making it less suited for treatment (Figs. 2 and 6). This is contrary to results obtained by Müller et al. for their folic acid targeted ^{177}Lu-labeled compound [16], and highlights that addition of an albumin binder does not always modify pharmacokinetics favourably [21]. Since in the clinic perfusion of cationic amino acids can reduce kidney uptake of radiolabeled somatostatin analogues, the same technique will need to be investigated with albumin-binder bearing somatostatin analogues to see if that technique can negate the increased kidney uptake and yield a therapeutic index that would be better than the reference compound. However, this does not address bone marrow uptake which is also higher in radiopharmaceuticals that have albumin-binding moieties and which is unlikely to benefit as much from the cationic amino-acids. It must be considered that hematopoietic toxicity may become the dose-limiting organ for that class of radiopharmaceutical with longer blood residence time.

Recently, Chen et al. appended a truncated Evans Blue (EB) analogue with the DOTATATE sequence, to develop an ^{86}Y/^{90}Y theranostic pair targeting SSTR2 [22]. The novel EB-octreotide derivative was able to achieve tumour uptake values of ~60%ID/g in AR42J tumours 24 h p.i. The [^{90}Y]Y-EB-TATE was able to significantly inhibit tumour growth and prolong survival in xenograft mice. This suggests the choice of albumin binder can greatly impact tumour uptake and corresponding target to non-target ratios. The choice of albumin binder moieties can change blood retention time significantly because of differing affinities for plasma albumin. Our choice of albumin binder increased circulation time moderately, but did not yield as high tumour uptake as those with longer half-life presented in the literature [22]. Modest increases in tumour uptake compared with tracers developed by Chen et al. that used similar techniques could also be secondary to different internalization behaviors because of the added albumin-binding motifs which would impact uptake at later time-points significantly. The same research group evaluated [^{177}Lu]Lu-DOTA-EB-TATE in small cohort of patients with advanced metastatic NETs with promising results [23]. [^{177}Lu]Lu-DOTA-EB-TATE was able to deliver 7.9 fold higher tumour dose compared to [^{177}Lu]Lu-DOTATATE, but this was also accompanied with 3.2 and 18.2 fold dose increase for kidneys and bone marrow respectively.

Interestingly, the addition of our albumin binders to [^{177}Lu]Lu-DOTATATE, decreased pancreas, adrenal, and lung uptake significantly; those tissues are known to normally express SST receptors [24,25]. It is possible that the addition of an albumin binding moiety has altered the affinity profile for other SSTR receptors, thought this would require further investigation.

5. Conclusion

Addition of an albumin binder to [^{177}Lu]Lu-DOTATATE increased blood residence time and tumour uptake, however the increase in kidney uptake was proportionally higher, thus reducing the therapeutic index and clinical usefulness. This is contrary to results published by

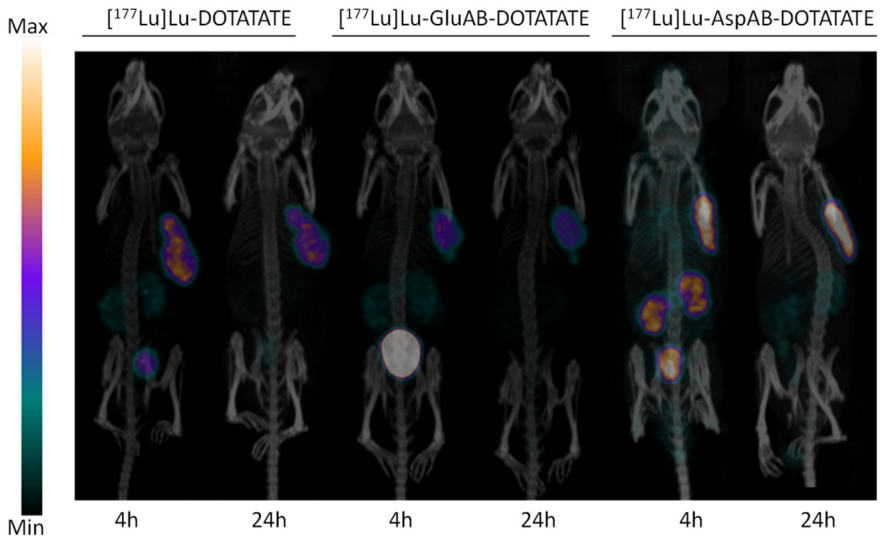

Fig. 6. SPECT/CT maximum intensity projections for [^{177}Lu]Lu-DOTATATE, [^{177}Lu]Lu-GluAB-DOTATATE, and [^{177}Lu]Lu-AspAB-DOTATATE acquired at 4 h and 24 h post-injection. Mice were intravenously injected with 39.2 ± 4.65 MBq of activity. Mice were anesthetized with inhalant isoflurane and scanned for either 30 (for 4 h time point) or 60 min (for 24 h time point).

other groups and demonstrates that addition of albumin-binding moieties can be deleterious for therapeutic index.

Conflict of interest

The authors declare no conflict of interest.

Acknowledgments

We would like to thank Helen Merkens for her technical expertise that proved invaluable in the experiments reported in this paper. Funding for these experiments was provided by the Canadian Institutes of Health Research (FDN-148465) and the BC Leading Edge Endowment Fund.

Appendix A. Supplementary data

Supplementary data to this article can be found online at https://doi.org/10.1016/j.nucmedbio.2018.08.001.

References

[1] Oberndorfer S. Karzinoide Tumoren des Dunndarms. Frankf Z Pathol 1907;1:426–9.
[2] Modlin IM, Kidd M, Latich I, Zikusoka MN, Shapiro MD. Current status of gastrointestinal carcinoids. Gastroenterology 2005;128:1717–51.
[3] Yao JC, Hassan M, Phan A, Dagohoy C, Leary C, Mares JE, et al. One hundred years after "carcinoid": epidemiology of and prognostic factors for neuroendocrine tumors in 35,825 cases in the United States. J Clin Oncol 2008;26:3063–72.
[4] Hallet J, How Lim Law C, Cukier M, Saskin R, Liu N, Singh S. Exploring the rising incidence of neuroendocrine tumors: a population-based analysis of epidemiology, metastatic presentation, and outcomes. Cancer 2015;121:589–97.
[5] Del Prete M, Buteau F-A, Beauregard J-M. Personalized ^{177}Lu-octreotate peptide receptor radionuclide therapy of neuroendocrine tumours: a simulation study. Eur J Nucl Med Mol Imaging 2017:1–11.
[6] Zaknun JJ, Bodei L, Mueller-Brand J, Pavel ME, Baum RP, Hörsch D, et al. The joint IAEA, EANM, and SNMMI practical guidance on peptide receptor radionuclide therapy (PRRNT) in neuroendocrine tumours. Eur J Nucl Med Mol Imaging 2013;40:800–16.
[7] Gulenchyn KY, Yao X, Asa SL, Singh S, Law C. Radionuclide therapy in neuroendocrine tumours: a systematic review. Clin Oncol 2012;24:294–308.
[8] Dalm SU, Nonnekens J, Doeswijk GN, de Blois E, van Gent DC, Konijnenberg MW, et al. Comparison of the therapeutic response to treatment with a ^{177}Lu-labeled somatostatin receptor agonist and antagonist in preclinical models. J Nucl Med 2016;57:260–5.
[9] Bhandari S, Watson N, Long E, Sharpe S, Zhong W, Xu S-Z, et al. Expression of somatostatin and somatostatin receptor subtypes 1–5 in human normal and diseased kidney. J Histochem Cytochem 2008;56:733–43.
[10] Bates CM, Kegg H, Grady S. Expression of somatostatin receptors 1 and 2 in the adult mouse kidney. Regul Pept 2004;119:11–20.
[11] Melis M, Krenning EP, Bernard BF, de Visser M, Rolleman E, de Jong M. Renal uptake and retention or radiolabeled somatostatin, bombesin, neurotensin, minigastrin and CCK analogues: species and gender differences. Nucl Med Biol 2007;34:633–41.
[12] Barone R, Van Der Smissen P, Devuyst O, Beaujean V, Pauwels S, Courtoy PJ, et al. Endocytosis of the somatostatin analogue, octreotide, by the proximal tubule-derived opossum kidney (OK) cell line. Kidney Int 2005;67:969–76.
[13] Rolleman EJ, Valkema R, de Jong M, Kooij PPM, Krenning EP. Safe and effective inhibition of renal uptake of radiolabelled octreotide by a combination of lysine and arginine. Eur J Nucl Med Mol Imaging 2003;30:9–15.
[14] Esser JP, Krenning EP, Teunissen JJM, Kooij PPM, van Gameren ALH, Bakker WH, et al. Comparison of [^{177}Lu-DOTA0,Tyr3]octreotate and [^{177}Lu-DOTA0,Tyr3]octreotide: which peptide is preferable for PRRT? Eur J Nucl Med Mol Imaging 2006;33:1346–51.
[15] Liu Z, Chen X. Simple bioconjugate chemistry serves great clinical advances: albumin as a versatile platform for diagnosis and precision therapy. Chem Soc Rev 2016;45:1432–56.
[16] Muller C, Struthers H, Winiger C, Zhernosekov K, Schibli R. DOTA conjugate with an albumin-binding entity enables the first folic acid-targeted ^{177}Lu-radionuclide tumor therapy in mice. J Nucl Med 2013;54:124–31.
[17] Dude I, Zhang Z, Rousseau J, Hundal-Jabal N, Colpo N, Merkens H, et al. Evaluation of agonist and antagonist radioligands for somatostatin receptor imaging of breast cancer using positron emission tomography. EJNMMI Radiopharm Chem 2017;2:4.
[18] Stabin MG, Sparks RB, Crowe E. OLINDA/EXM: the second-generation personal computer software for internal dose assessment in nuclear medicine. J Nucl Med 2005;46:1023–7.
[19] Keenan MA, Stabin MG, Segars WP, Fernald MJ. RADAR realistic animal model series for dose assessment. J Nucl Med 2010;51:471–6.
[20] Stabin MG, Konijnenberg MW. Re-evaluation of absorbed fractions for photons and electrons in spheres of various sizes. J Nucl Med 2000;41:149–60.
[21] Benesova M, Umbricht CA, Schibli R, Muller C. Albumin-binding PSMA ligands: optimization of the tissue distribution profile. Mol Pharm 2018;15:934–46.
[22] Tian R, Jacobson O, Niu G, Kiesewetter DO, Wang Z, Zhu G, et al. Evans blue attachment enhances somatostatin receptor subtype-2 imaging and radiotherapy. Theranostics 2018;8:735–45.
[23] Zhang J, Wang H, Jacobson Weiss O, Cheng Y, Niu G, Li F, et al. Safety, pharmacokinetics and dosimetry of a long-acting radiolabeled somatostatin analogue (177)Lu-DOTA-EB-TATE in patients with advanced metastatic neuroendocrine tumors. J Nucl Med 2018 Apr 13. https://doi.org/10.2967/jnumed.118.209841 [Epub ahead of print].
[24] Reubi JC, Kvols L, Krenning E, Lamberts SWJ. Distribution of somatostatin receptors in normal and tumor tissue. Metabolism 1990;39:78–81.
[25] Rohrer L, Raulf F, Bruns C, Buettner R, Hofstaedter F, Schüle R. Cloning and characterization of a fourth human somatostatin receptor (GTP-binding-protein-coupled receptor/somatostatin receptor gene). Biochemistry 1993;90:4196–200.